

# Vibration Suppression Control Profile Generation with Both Acceleration and Velocity Constraints

Li Zhou and Eduardo A. Misawa

**Abstract**—A control profile is generated which suppresses all the resonant dynamics in a flexible dynamic system. This control profile has both the acceleration and velocity constraints. The control profile is generated from the time-optimal acceleration command and the vibration suppression shape filter technology. The simulation results for hard disk drive long seek control show the effectiveness of the proposed method.

## I. INTRODUCTION

Control of flexible structures has been extensively studied in recent years. Flexible structures such as high-speed disk drive actuators require extremely precise positioning under very tight time constraints. Whenever a fast motion is commanded, residual vibration in the flexible structure is induced, which increases the settling time. One solution is to design a closed-loop controller to damp out vibrations caused by the command inputs and disturbances to the plant. However, the resulting closed-loop response may still be too slow to provide an acceptable settling time, and the closed-loop control is not able to compensate for high frequency residual vibration which occurs beyond the closed-loop bandwidth. An alternative approach is to develop an appropriate reference trajectory that is able to minimize the excitation energy imparted to the system at its natural frequencies.

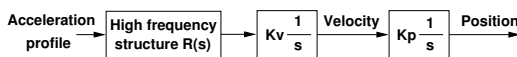


Fig. 1. A typical mechanical flexible system.

Fig. 1 shows a typical mechanical flexible system, where  $\frac{1}{s}$  is an integrator,  $K_v$  is a velocity constant gain, and  $K_p$  is a position constant gain. The high frequency modes can be described as a transfer function  $R(s) = \lim_{n \rightarrow \infty} \frac{b_n s^n + b_{n-1} s^{n-1} + \dots + b_1 s + 1}{a_n s^n + a_{n-1} s^{n-1} + \dots + a_1 s + 1}$  in which an infinite number of lightly damped resonant structures is possible. The goal of vibration suppression trajectory generation is to find a fast input trajectory, under some physical constraint, with minimum possible residual vibration.

This work was supported by the National Science Foundation, grant number 9978748, and Seagate Technology LLC of Oklahoma City, Oklahoma.

L. Zhou is with the School of Mechanical and Aerospace Engineering, Oklahoma State University, Stillwater, OK 74078-5016, USA  
zhou1@acl.okstate.edu

E. A. Misawa is with Faculty of School of Mechanical and Aerospace Engineering, Oklahoma State University, Stillwater, OK 74078-5016, USA  
misawa@ceat.okstate.edu

In the previous study [1], [2], a control profile is generated which suppresses all the resonant dynamics in a flexible dynamic system. The proposed methods [1], [2] develop a vibration suppression control profile in the hard disk drive short seek control. However, for hard disk drive long seek control, both acceleration (or drive current) and velocity constraints should be considered. The vibration suppression control profile generation with both acceleration and velocity constraints is studied in this paper.

The paper is organized as follows. Section II describes the time-optimal control profile with velocity constraint. Section III then develops vibration suppression control profile generation with both acceleration and velocity constraints for a flexible system. Next, simulation results for a hard disk drive open-loop long seek control are presented in section IV. The paper closes with conclusions.

## II. TIME-OPTIMAL CONTROL PROFILE WITH VELOCITY CONSTRAINT

The famous Bang-Bang Principle was explained by Hermes [3] as: “It had been an intuitive assumption for some time that if the control for a system is operating from a limited source of power and if it is desired to have the system change from one state to another in minimum time, then it is necessary at all times to utilize all the power available; that is, to use bang-bang control.” With the Bang-Bang Principle, the time-optimal commands must be piecewise constant functions of time and the constants are solely determined by the actuator maximum and minimum power limits. That means the time-optimal control must always saturate the actuators.

For a purely rigid body, it can be inferred that the time-optimal acceleration profile is composed by two parts. The first part is an acceleration command which always reaches the maximum limit and the second part is a deceleration command which always reaches the minimum limit. Fig. 2 shows typical time-optimal control profiles with acceleration constraint. If there is also a velocity limit for the rigid body movement, it can be inferred that the time-optimal acceleration profile is composed by three parts. First, acceleration is commanded which always reaches the maximum limit. Secondly, when the maximum velocity is reached, the acceleration command becomes zero. In this situation, the rigid body is cruising with a constant velocity. The third part is a deceleration command which always reaches the minimum limit. Fig. 3 shows typical time-optimal control profiles with both acceleration and velocity constraints. From the previous study [1], the time-optimal

command has a poor energy concentration property so it is not suitable to suppress all the resonant dynamics in a flexible system.

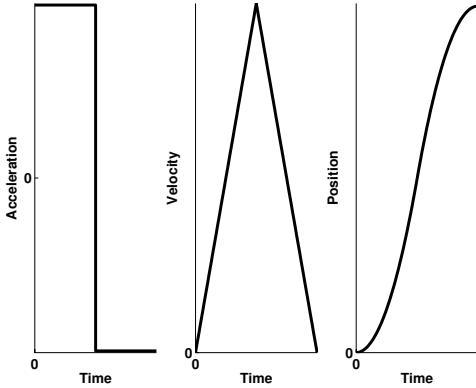


Fig. 2. Time-Optimal control profiles with acceleration constraint.

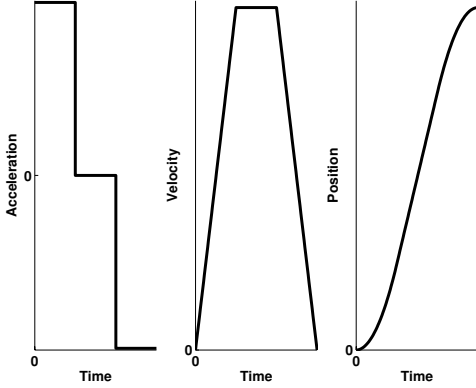


Fig. 3. Time-Optimal control profiles with both acceleration and velocity constraints.

### III. VIBRATION SUPPRESSION CONTROL PROFILE GENERATION WITH BOTH ACCELERATION AND VELOCITY CONSTRAINTS FOR A FLEXIBLE SYSTEM

In this section, a vibration suppression control profile generation with both acceleration and velocity constraints for a flexible system is induced by using the vibration suppression shape filter technique [4], [5].

#### A. Calculating the Number of the Time-Optimal Positive Acceleration Command Samples to Reach the Velocity Constraint

In this section, the number of the time-optimal positive acceleration command samples is calculated. The constraint of the acceleration  $u[k]$  is assumed to be  $|u[k]| \leq A_{max}$ . The maximum velocity is assumed to be  $V_{max}$  and the sampling period is assumed to be  $T_s$ . The relationship between the acceleration command  $u[k]$  and the velocity  $v[k]$  is given as  $\frac{V(z)}{U(z)} = K_a \frac{z^{-1}}{1-z^{-1}}$ , where  $K_a$  is a constant gain. The difference equation between acceleration  $u[k]$

at the discrete-time instant  $kT_s$  and velocity  $v[k]$  at the discrete-time instant  $kT_s$  is given as

$$v[k] = K_a u[k-1] + v[k-1]. \quad (1)$$

If the initial velocity  $v[0]$  is assumed to be zero, the velocity at the discrete-time instant  $kT_s$  can be computed as

$$v[k] = K_a \sum_{i=0}^{k-1} u[i]. \quad (2)$$

Since the acceleration  $u[k]$  always saturates before reaching the maximum velocity, the positive acceleration command  $u[k]$  is described as  $u[k] = A_{max}$ ,  $k = 0, \dots, m-1$ . As a result the following equation holds,

$$V_{max} = K_a \sum_{i=0}^{m-1} u[i] = K_a m A_{max}. \quad (3)$$

The number of the time-optimal positive acceleration command samples can be calculated as

$$m_1 = \text{floor} \left( \frac{V_{max}}{K_a A_{max}} \right) \quad (4)$$

and the maximum velocity  $V_{rmax}$  from (4) is

$$V_{rmax} = K_a m_1 A_{max} \leq V_{max}. \quad (5)$$

#### B. Calculating the Number of the Time-Optimal Zero Acceleration Command Samples

When the rigid body reaches the maximum velocity constraint described in (5), the rigid body is cruising at the constant velocity  $V_{rmax}$  as shown in Fig. 3. If the position movement is assumed to be  $P_{max}$ , the number of the time-optimal zero acceleration command samples is calculated. The state-space model of the rigid body is described as

$$\begin{bmatrix} p[k+1] \\ v[k+1] \end{bmatrix} = G \begin{bmatrix} p[k] \\ v[k] \end{bmatrix} + K_b H u[k], \quad (6)$$

where  $G = \begin{bmatrix} 1 & T_s \\ 0 & 1 \end{bmatrix}$ ,  $H = \begin{bmatrix} T_s^2/2 \\ T_s \end{bmatrix}$ ,  $p[k]$  is the position at the discrete-time instant  $kT_s$ ,  $v[k]$  is the velocity at the discrete-time instant  $kT_s$ , and  $K_b$  is a constant gain. The acceleration command  $u$  has the following format

$$u = [\underbrace{A_{max}, \dots, A_{max}}_{m_1}, \underbrace{0, \dots, 0}_n, \underbrace{-A_{max}, \dots, -A_{max}}_{m_1}].$$

If the initial position  $p[0]$  and velocity  $v[0]$  are assumed to be zero, the position and velocity at the discrete-time instant  $kT_s$  can be computed as [6]

$$\begin{bmatrix} p[k] \\ v[k] \end{bmatrix} = G^k \begin{bmatrix} p[0] \\ v[0] \end{bmatrix} + \sum_{i=0}^{k-1} G^i K_b H u[k-i-1], \quad (7)$$

$$= \sum_{i=0}^{k-1} G^i K_b H u[k-i-1]. \quad (8)$$

So at the discrete-time instant  $(2m_1 + n)T_s$ ,

$$\begin{bmatrix} p[2m_1 + n] \\ v[2m_1 + n] \end{bmatrix} = \sum_{i=0}^{2m_1+n-1} G^i K_b H u[2m_1 + n - i - 1], \quad (9)$$

$$= K_b A_{max} \begin{bmatrix} T_s^2 m_1 (m_1 + n) \\ 0 \end{bmatrix}. \quad (10)$$

If the position at the discrete-time instant  $(2m_1 + n)T_s$  is imposed to be  $P_{max}$ , then

$$K_b A_{max} T_s^2 m_1 (m_1 + n) = P_{max} \quad (11)$$

and

$$n = \frac{P_{max}}{K_b A_{max} T_s^2 m_1} - m_1. \quad (12)$$

Generally the above  $n$  is not an integer. Let  $n = \text{floor}(n) + \alpha$ , where  $\alpha = n - \text{floor}(n)$  and  $0 \leq \alpha < 1$ . The number of zero acceleration command samples can be chosen to be

$$n_1 = \text{floor}(n) + 1. \quad (13)$$

In the above implementation, since the resultant number of zero acceleration command  $n_1$  is generally greater than the required fractional number of samples  $n$ , the resultant position at the end of the acceleration command is greater than the required position constraint which is  $P_{max}$ . Fig. 4 shows the fractional number of the maximum velocity profile. The time interval between the final maximum velocity impulse  $V_{rmax}$  and the next velocity impulse  $b_0$  is  $\alpha T_s$  which is less than one sampling period  $T_s$ . Fig. 5 shows the modification of the integer number of the maximum velocity profile from (13). Compared with Fig. 4, the summation of velocity impulses in Fig. 5 is increased by  $(1 - \alpha)V_{rmax}$  per sample. The additional velocity impulse summation can be compensated for by slightly modifying the velocity impulses. The acceleration command corresponding the velocity profile in Fig. 5 is

$$u = \underbrace{[A_{max}, \dots, A_{max}]}_{m_1}, \underbrace{[0, \dots, 0]}_{n_1}, \underbrace{[-A_{max}, \dots, -A_{max}]}_{m_1}. \quad (14)$$

The velocity profile from (14) can be described as

$$\begin{aligned} v[0] &= 0, \\ v[1] &= K_a A_{max}, \\ v[k] &= K_a \sum_{i=0}^{k-1} u[i], k = 2, \dots, 2m_1 + n_1 - 2 \end{aligned}$$

$$v[2m_1 + n_1 - 1] = K_a A_{max},$$

$$v[2m_1 + n_1] = 0.$$

The above velocity profile can be modified to

$$\begin{aligned} v_1[0] &= 0, \\ v_1[k] &= v[k] - \frac{(1 - \alpha)V_{rmax}}{2m_1 + n_1 - 1}, \\ k &= 1, \dots, 2m_1 + n_1 - 1, \\ v_1[2m_1 + n_1] &= 0. \end{aligned}$$

The integral of the modified velocity impulses is exactly the same as the required integral of the velocity impulses in Fig. 4. The resultant modified acceleration command corresponding to (14) is

$$\begin{aligned} u_1[0] &= A_{max} - \frac{(1 - \alpha)V_{rmax}}{K_a(2m_1 + n_1 - 1)}, \\ u_1[k] &= u[k], k = 1, \dots, 2m_1 + n_1 - 1, \\ u_1[2m_1 + n_1 - 1] &= - \left[ A_{max} - \frac{(1 - \alpha)V_{rmax}}{K_a(2m_1 + n_1 - 1)} \right]. \end{aligned} \quad (15)$$

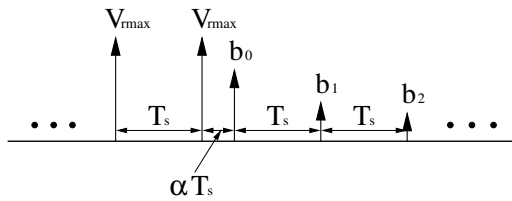


Fig. 4. The calculated fractional number of the maximum velocity profile.

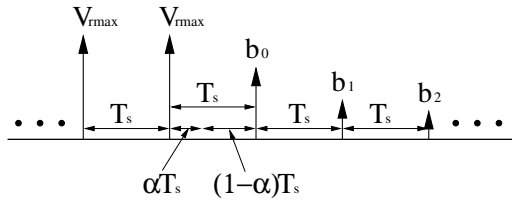


Fig. 5. The modification of the integer number of the maximum velocity profile.

In (13), if the resultant integer number  $n_1$  of the zero acceleration command is less than 0, then the acceleration and the velocity limits are not required to achieve the position constraint. In this situation, to guarantee the position constraint, either a reduced acceleration limit or a reduced velocity limit may be implemented. It is easy to understand that the resultant maximum velocity from the modified acceleration command (15) is slightly less than  $V_{rmax}$  in (5).

#### C. Vibration Suppression Control Profile Generation with Both Acceleration and Velocity Constraints

Since the time-optimal acceleration command is generated in the previous sections, a vibration suppression command can be generated as shown in Fig. 6. The vibration suppression command is the convolution of the time-optimal command and the vibration suppression shape filter. The vibration suppression shape filter in Fig. 6 is simply described in [4], [5]. In [4], it shows that both the Input Shaping<sup>®</sup> [7], [8] and OATF [9], [10] are special cases of a non-continuous function based vibration suppression shape filter. Different from the Input Shaping<sup>®</sup> and OATF,

<sup>1</sup>Input Shaping<sup>®</sup> is a registered trademark of Convolve, Inc. in the United States.

the vibration suppression shape filter in [4] is generated from a continuous function, so it is able to suppress the high frequency resonance modes besides canceling the low frequency resonance modes if the shape filter is designed based on a low frequency resonance mode. However, the Input Shaping<sup>®</sup> and OATF are not able to suppress the unmodeled high frequency vibrations if they are designed based on a low frequency resonance mode [4].



Fig. 6. Generation of a vibration suppression command.

#### IV. SIMULATION RESULTS FOR HARD DISK DRIVE LONG SEEK CONTROL

Consider the following flexible system which is embedded in a hard disk assembly,  $H(s) = K_c \cdot K_v \cdot K_p \cdot R(s) \frac{1}{s^2}$ , where the input is the current signal in amps and the output is the position signal in tracks. The variable  $K_c = 1.3 \frac{\text{tracks/sample}^2}{\text{amp}}$  is a constant gain from current to acceleration,  $K_v = 5 \times 10^4 \frac{\text{samples}}{\text{sec}}$  is the velocity gain,  $K_p = 5 \times 10^4 \frac{\text{sec}}{\text{samples}}$  is the position gain, and  $R(s)$  is a resonance structure. The Bode magnitude plot of a reduced order (28<sup>th</sup>)  $R(s)$  is shown in Fig. 7. This resonance transfer function  $R(s)$  was derived from the flexible arm of an open disk drive at the Oklahoma State University Advanced Controls Laboratory. The resonance modes change drastically due to variation of the mode parameters. On the Bode plot, the peaks of the frequency response may shift both in frequency and in amplitude.

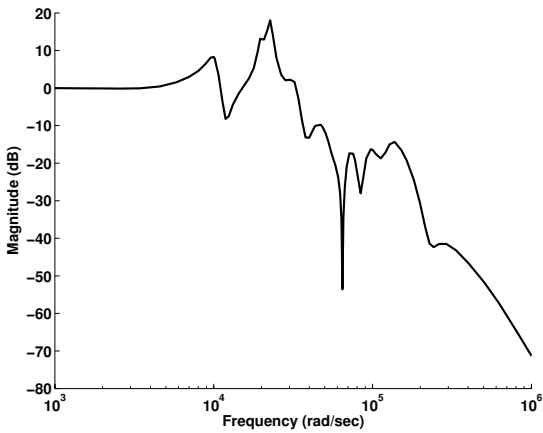


Fig. 7. Bode magnitude of the resonance structure.

The current limit is assumed to be 1 amp, the maximum velocity constraint is assumed to be 100 tracks/sample, and the long seek position movement is assumed to be  $2 \times 10^5$  tracks. The sampling period  $T_s$  is assumed to be  $2 \times 10^{-5}$  seconds. Fig. 8 shows the time-optimal current command with the velocity constraint. Fig. 9 shows the resultant

velocity signal. Fig. 10 shows the resultant position signal. Fig. 11 shows the position signal near the target track. The interval of Y axis in Fig. 11 is scaled to exactly one track and it shows that the residual vibration exists for a long period of time after the end of the current command (5.6 msec).

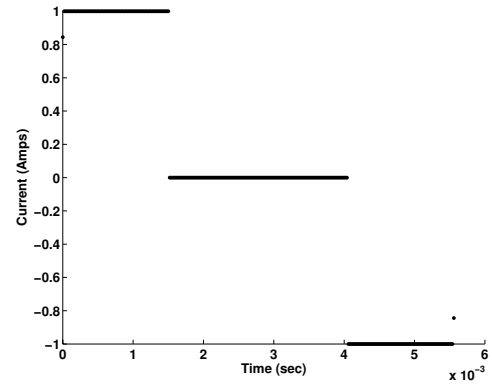


Fig. 8. Time-Optimal current command with the velocity constraint.

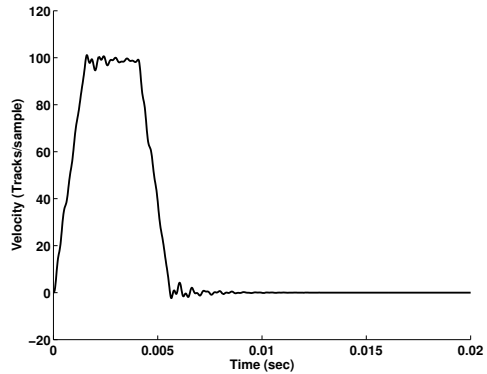


Fig. 9. The velocity signal with the time-optimal current command.

To suppress the residual vibration, a rectangle based shaper filter [4] is designed based on the first resonance mode in the flexible system. The first resonance mode has the parameter  $\omega_1 = 6.12 \times 10^3 \text{ rad/sec}$  and  $\zeta_1 = 0.7$ . Fig. 12 shows the resultant vibration suppression shape filter. Fig. 13 shows the vibration suppression current command. Fig. 14 shows the resultant velocity signal. Fig. 15 shows the resultant position signal near the target track. Although the residual vibration due to the first resonance mode has been canceled, a large vibration still exists after the end of the current command. This residual vibration is caused by the second resonance mode in the flexible system.

To suppress the residual vibration of the second resonance mode, a rectangle based shaper filter [4] is designed based on the second resonance mode in the flexible system. This mode has the parameter  $\omega_1 = 1.02 \times 10^4 \text{ rad/sec}$  and  $\zeta_1 = 0.08$ . Fig. 16 shows the resultant vibration suppression shape filter based on the second resonance mode. Combining the shape filter in Fig. 12 and the shape

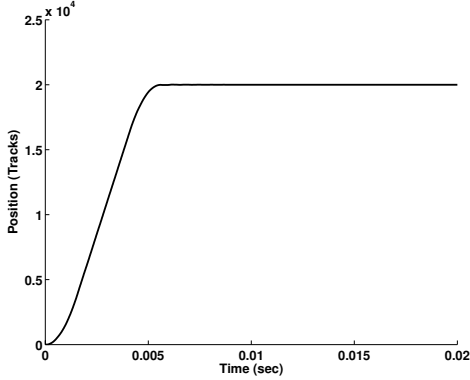


Fig. 10. The position signal with the time-optimal current command.

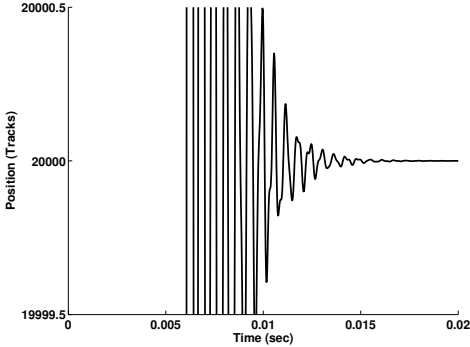


Fig. 11. The position signal near the target track.

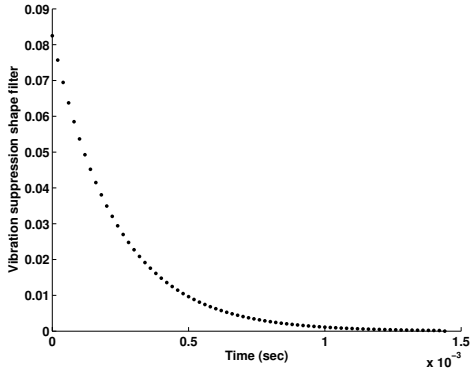


Fig. 12. Rectangle based shape filter based on resonance parameter  $\omega_1 = 6.12 \times 10^3$  rad/sec and  $\zeta_1 = 0.7$ .

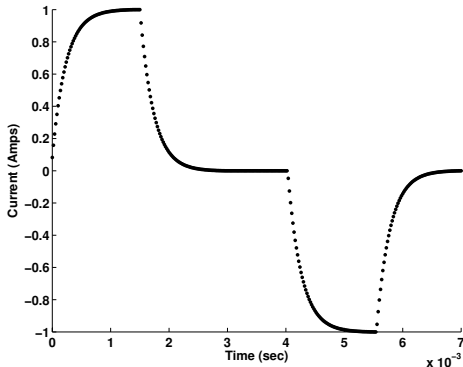


Fig. 13. Vibration suppression current command.

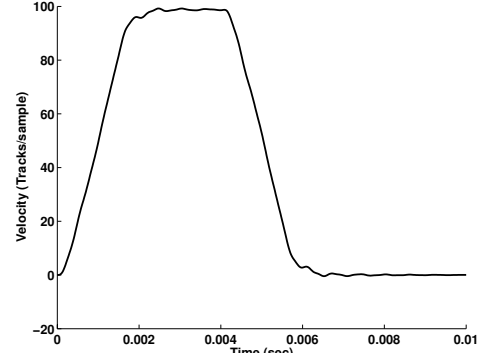


Fig. 14. Velocity signal with the vibration suppression current command.

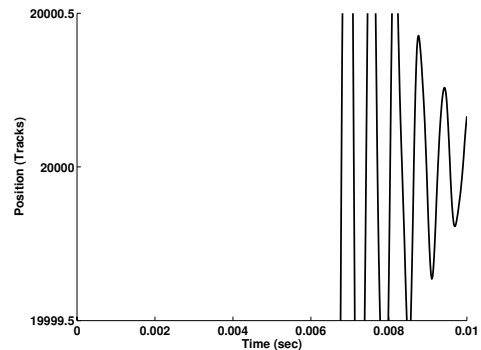


Fig. 15. Position signal near the target track.

filter in Fig. 16 results in a new shape filter as shown in Fig. 17. The resultant new vibration suppression shape filter in Fig. 17 cancels the residual vibration due to both the first and the second resonance modes. Fig. 18 shows the vibration suppression current command. Fig. 19 shows the resultant velocity signal. Fig. 20 shows the resultant position signal near the target track. It is obvious that the residual vibration due to both the first and the second resonance modes is canceled and the residual vibration due to the high frequency modes is also suppressed. In this case, it is not necessary to design a high frequency vibration suppression shape filter [5] to suppress all the high frequency residual vibration because the high frequency vibration is sufficiently suppressed by the two rectangle based shape filters.

## V. CONCLUSIONS

In this examination, a vibration suppression control profile is generated with both the acceleration and velocity constraints. The simulation results of the hard disk drive long seek control show the effectiveness of this method. The proposed methods apply to other flexible dynamic system long seek control problems.

The methods in this paper are patented (pending). Commercial use of these methods requires written permission from the Oklahoma State University.

The authors would like to thank Matthew Duvall for useful discussions.

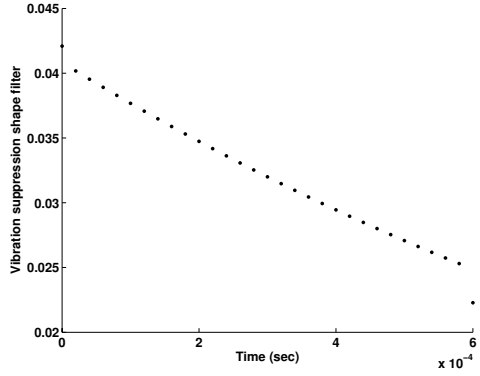


Fig. 16. Rectangle based shape filter based on resonance parameter  $\omega_2 = 1.02 \times 10^4$  rad/sec and  $\zeta_1 = 0.08$ .

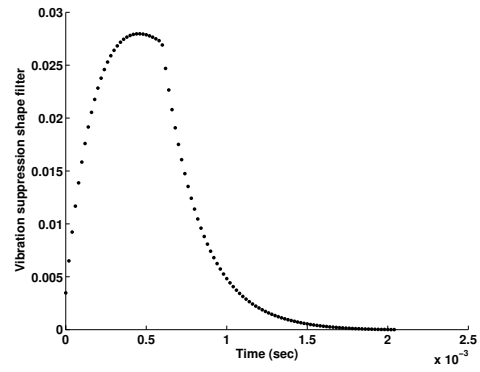


Fig. 17. Vibration suppression shape filter to cancel both the first resonance mode and the second resonance mode.

## REFERENCES

- [1] L. Zhou and E. A. Misawa, "Robust vibration suppression control profile generation based on time-frequency uncertainty," in *Proceedings of the American Control Conference*, Boston, MA, 2004.
- [2] ———, "Generation of a robust vibration suppression control profile from optimal energy concentration functions," accepted to the 2005 American Control Conference, Portland, OR.
- [3] H. Hermes and J. P. LaSalle, *Functional Analysis and Time Optimal Control*. Academic Press, New York, 1969.
- [4] L. Zhou and E. A. Misawa, "From Input Shaping® and OATF to vibration suppression shape filter," accepted to the 2005 American Control Conference, Portland, OR.
- [5] ———, "Low frequency vibration suppression shape filter and high frequency vibration suppression shape filter," accepted to the 2005 American Control Conference, Portland, OR.
- [6] K. Ogata, *Discrete-Time Control Systems*. Prentice Hall, Inc., Englewood Cliffs, NJ, 1995.
- [7] N. C. Singer, "Residual vibration reduction in computer controlled machines," Ph.D. dissertation, Massachusetts Institute of Technology, 1988.
- [8] N. C. Singer, W. P. Seering, and K. A. Pasch, "Shaping command inputs to minimize unwanted dynamics," United States Patent, 4,916,635, April 1990.
- [9] D. P. Magee and W. J. Book, "Optimal filtering to minimize the elastic behavior in serial link manipulators," in *Proceedings of the American Control Conference*, vol. 1, 1998, pp. 2637–2641.
- [10] ———, "Optimal arbitrary time-delay (OAT) filter and method to minimize unwanted system dynamics," United States Patent, 6,078,844, June 2000.

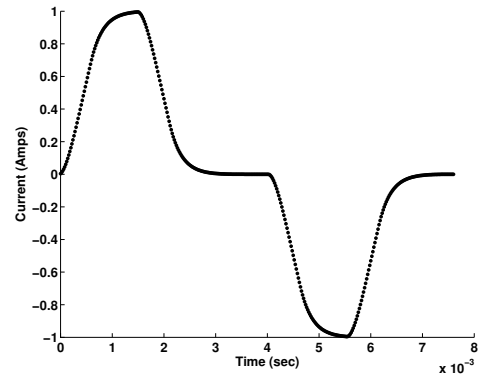


Fig. 18. Vibration suppression current command.

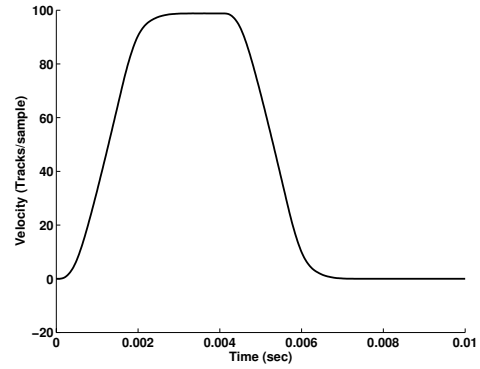


Fig. 19. Velocity signal with the vibration suppression current command.

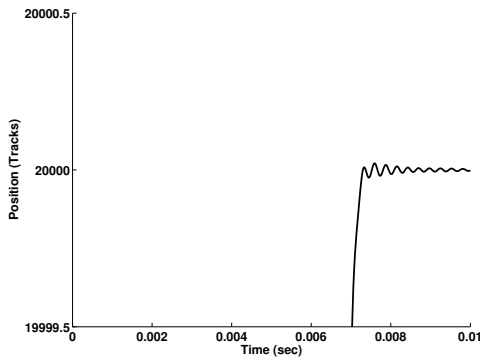


Fig. 20. Position signal near the target track.